

Conformal prediction for high-dimensional functional time series: Applications to subnational mortality

Han Lin Shang 

Department of Actuarial Studies and Business Analytics

Macquarie University

Abstract

In statistics, forecast uncertainty is often quantified using a specified statistical model, though such approaches may be vulnerable to model misspecification, selection bias, and limited finite-sample validity. While bootstrapping can potentially mitigate some of these concerns, it is often computationally demanding. Instead, we take a model-agnostic and distribution-free approach, namely conformal prediction, to construct prediction intervals in high-dimensional functional time series. Among a rich family of conformal prediction methods, we study split and sequential conformal prediction. In split conformal prediction, the data are divided into training, validation, and test sets, where the validation set is used to select optimal tuning parameters by calibrating empirical coverage probabilities to match nominal levels; after this, prediction intervals are constructed for the test set, and their accuracy is evaluated. In contrast, sequential conformal prediction removes the need for a validation set by updating predictive quantiles sequentially via an autoregressive process. Using subnational age-specific log-mortality data from Japan and Canada, we compare the finite-sample forecast performance of these two conformal methods using empirical coverage probability and the mean interval score.

Keywords: coverage calibration; forecast uncertainty quantification; functional panel data; split conformal prediction; sequential conformal prediction

*Corresponding address: Department of Actuarial Studies and Business Analytics, Level 7, 4 Eastern Road, Macquarie University, Sydney, NSW 2109, Australia. Email: hanlin.shang@mq.edu.au

1 Introduction

A fundamental problem in modeling and forecasting time series of random functions or objects is quantifying forecast uncertainty. Such an uncertainty is often manifested probabilistically through the construction of pointwise prediction intervals or uniform prediction bands. The prediction interval or band allows one to assess future uncertainty levels, plan different strategies for a range of possible outcomes indicated by the interval forecasts, compare forecasts from different methods more thoroughly, and explore different scenarios based on various assumptions (Chatfield, 2000). In the literature of functional time series, Paparoditis and Shang (2023) proposed a sieve bootstrap method to construct prediction bands. The sieve bootstrap generates stationary functional time series bootstrap samples and their forecasts via a vector autoregression representation, and it can calibrate the model misspecification error, which does not vanish asymptotically.

While most of the existing literature focuses on a small (fixed) number of functional time series, it is increasingly common to collect large numbers of them across diverse fields. For instance, in climatology, temperature curves are routinely recorded in hundreds of weather stations; in finance, return curves are typically available for thousands of stocks. These applications are examples of high-dimensional functional time series (HDFTS), which have received increasing attention in recent years. A HDFTS can be denoted by $Z_{t,s}(\mathbf{u}), s = 1, \dots, N, t = 1, \dots, T$ with $Z_{t,s} = (Z_{t,s}(\mathbf{u}), \mathbf{u} \in \mathcal{C}_s) \in \mathcal{H}_s$, where \mathcal{H}_s is a Hilbert space defined as a set of measurable and square-integrable functions on a compact set \mathcal{C}_s . A distinct feature of HDFTS is that the number of cross sections can exceed the number of curves, i.e., $N > T$.

In the functional time series literature, the study of HDFTS is in its infancy. Hallin et al. (2023) presented a theoretical representation within a functional factor model framework, while Li et al. (2024) developed an information criterion for detecting and estimating change points, and clustering them into common change points. For estimating parameters in a HDFTS model, Tavakoli et al. (2023) proposed a functional factor model with functional factor loadings and real-valued factors, whereas Guo et al. (2026) derived a different factor model with real-valued factor loadings and functional factors; by unifying the two factor models, Leng et al. (2026) developed a unified factor model with functional factor loadings and functional factors. Because of cross-

sectional and temporal dependencies in the HDFTS, [Happ and Greven \(2018\)](#) combined principal component scores derived from different populations and subsequently performed a separate real-valued principal component analysis on the aggregated scores. [Gao et al. \(2019\)](#) adopted a two-stage procedure that integrates truncated functional principal component analysis with a scalar factor model applied to the resulting panel of scores. [Jiménez-Varón et al. \(2024\)](#) developed a two-way functional analysis of variance to decompose HDFTS into deterministic components, namely grand, row, and column effects, and time-varying residual processes.

To quantify forecast uncertainty, the main aim of this paper is to propose an approach for constructing prediction intervals for HDFTS using a conformal prediction approach. As computationally efficient algorithms, we extensively study split conformal prediction of [Lei et al. \(2018\)](#) and sequential conformal prediction of [Xu and Xie \(2023\)](#), both developed for distribution-shift time series. Between the two conformal prediction methods, we recommend the sequential conformal prediction, as it does not require parameter calibration using a validation set. To the best of our knowledge, this is the first study to examine forecast uncertainty under an HDFTS setting.

The remainder of the paper is outlined as follows. In [Section 2](#), we introduce a motivating example, namely Japanese subnational age- and sex-specific log mortality rates. [Section 3](#) presents two decompositions, namely one-way functional analysis of variance and functional factor model of [Leng et al. \(2026\)](#). Since both decompositions can exactly recover an HDFTS, there is no loss of information. In [Section 4](#), we present the two variants of conformal prediction, tailored for functional time series. In [Section 5](#), we describe the forecast evaluation setup and error metric. The interval forecast accuracy is evaluated and compared between the two variants of conformal predictions in [Section 6](#). [Section 7](#) concludes, along with some ideas on how the methodology can be further extended. In the Appendix, we present a robustness sensitivity analysis by applying the split and sequential conformal prediction methods to Canadian subnational age- and sex-specific mortality rates to further validate our results.

2 Japanese subnational age- and sex-specific mortality rates

We demonstrate the idea of conformal prediction using Japanese subnational age- and sex-specific mortality rates from 1975 to 2023, sourced from [Japanese Mortality Database \(2026\)](#). The original dataset captures mortality rates for both sexes at 47 prefectures, shown in Figure 1.



Figure 1: A map of 47 Japanese prefectures ordered geographically from the most northern region (Hokkaido) to the most southern region (Okinawa).

For analytical refinement, age groups have been aggregated to span 0-99 in a single year of age, with the last age group 100+. This aggregation helps generate a comprehensive overview of mortality trends while bypassing noisy data associated with extremely high ages. Because of measurement errors, observed subnational mortality rates are noisy across ages. We employed penalized regression spline smoothing with a monotonic constraint ([Wood, 1994](#)) at age 65 to generate smooth functions and to handle missing data and values outside the unit interval. In functional data analysis, it is often assumed that the log mortality rate in each year follows an underlying smooth function of age, $y_t(u)$, such that

$$\log \mathcal{Z}_t(u_j) = \log y_t(u_j) + \sigma_t(u_j)\epsilon_{t,j},$$

where $z_t(u_j)$ denotes the original mortality rate, and $y_t(u_j)$ denotes the smoothed mortality rate for $t = 1, \dots, T, j = 1, \dots, J$. The error term $\epsilon = (\epsilon_1, \dots, \epsilon_J), \epsilon_1 = (\epsilon_{1,1}, \dots, \epsilon_{T,1})^\top$ is independent and identically distributed variables with zero mean and unit variance, where J denotes the number of ages, and $\sigma_t(u_j)$ allows for heteroskedasticity. The smooth shape of age-specific mortality rates over age in each year is a distinguishing feature, which can improve short-term forecast accuracy (see, e.g., [Basellini and Camarda, 2019](#); [Yang et al., 2024](#)). Computationally, the `smooth.demogdata` function in the demography package ([Hyndman, 2025](#)) was used to smooth the raw data.

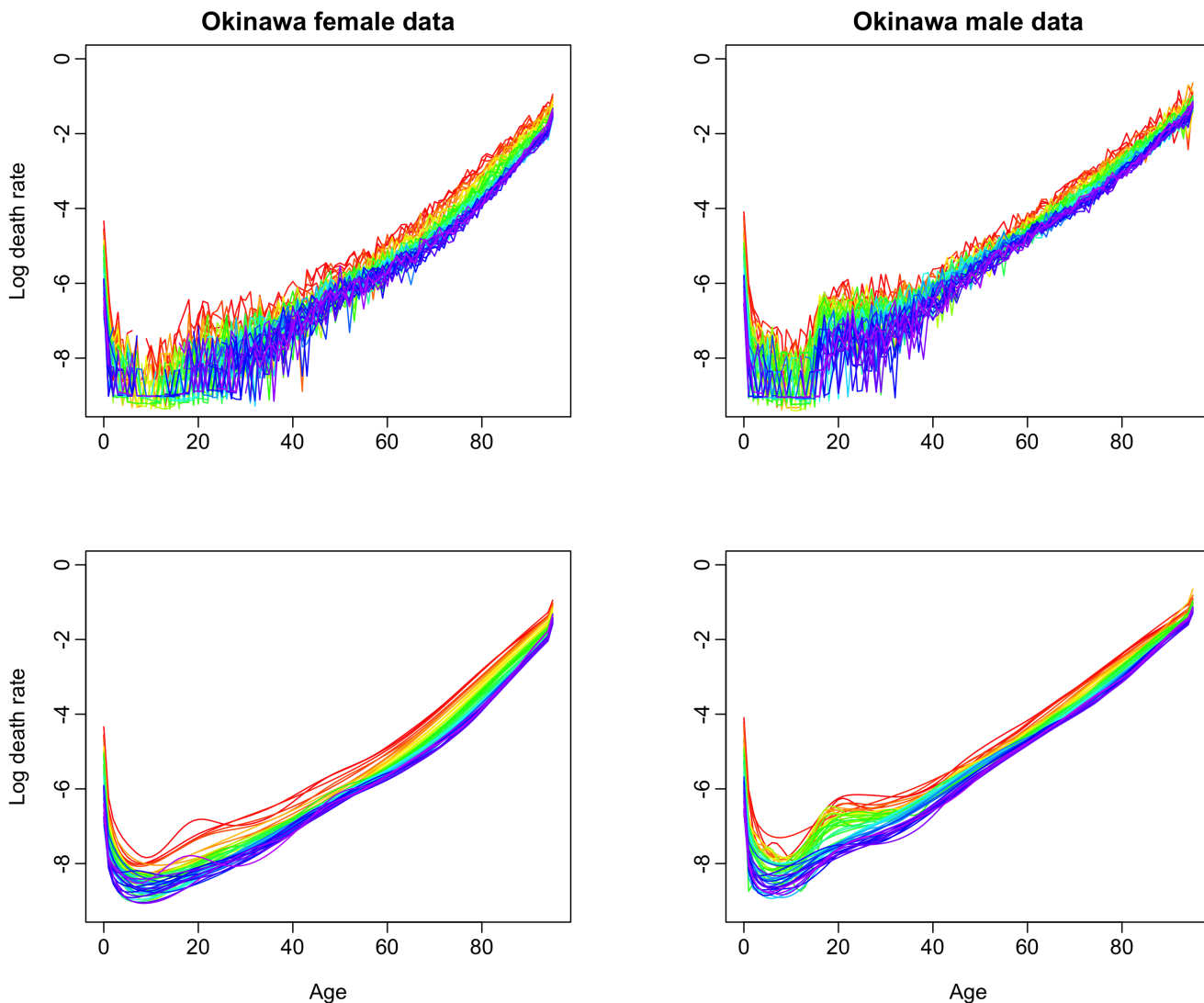


Figure 2: The raw (first row) and smoothed (second row) age-specific log mortality rates between 1975 and 2023 in Okinawa, Japan. Curves are ordered chronologically using a rainbow color palette; the oldest curves are shown in red, and the most recent in violet.

To visualize the time trend, we present the age-specific mortality rates using a rainbow plot of [Hyndman and Shang \(2010\)](#) in Figure 2. The log mortality rates from the distant past years

are shown in red, while data from the most recent years are shown in purple. The figures show typical mortality curves for a developed country, with rapidly decreasing mortality rates in the early years of life, followed by an increase during the teenage years, a plateau in young adulthood, and then a steady increase from about age 30 (see also [Jiménez-Varón et al., 2024](#)). By examining changes in mortality rates by age, year, and region, it becomes evident that mortality rates have undergone substantial variation over time. Like many developed nations, females generally have lower mortality rates than males at all ages in Japan. Since females and males are biologically different, we treat each of them separately.

3 Decomposition of high-dimensional functional time series

3.1 One-way functional analysis of variance

As we observe functional time series (i.e., log age-specific mortality rates) at each state, we are interested in examining the effect of the state, also known as the functional row effect. Let us denote

$$\begin{bmatrix} y_{1,1}(\mathbf{u}) & y_{2,1}(\mathbf{u}) & \cdots & y_{T,1}(\mathbf{u}) \\ y_{1,2}(\mathbf{u}) & y_{2,2}(\mathbf{u}) & \cdots & y_{T,2}(\mathbf{u}) \\ \vdots & \vdots & \ddots & \vdots \\ y_{1,47}(\mathbf{u}) & y_{2,47}(\mathbf{u}) & \cdots & y_{T,47}(\mathbf{u}) \end{bmatrix}.$$

We consider an exact decomposition, known as the one-way functional ANOVA (see, e.g., [Smaga, 2026](#); [Cuesta-Albertos and Febrero-Bande, 2010](#), p.538). The log mortality rates can be decomposed as

$$\log y_{t,s}(\mathbf{u}) = \underbrace{\theta(\mathbf{u}) + \delta_s(\mathbf{u})}_{\text{deterministic}} + \underbrace{\mathcal{X}_{t,s}(\mathbf{u})}_{\text{time-varying}},$$

where $\theta(\mathbf{u})$ represents a functional grand effect, $\delta_s(\mathbf{u})$ denotes the s^{th} functional row effect, and $\mathcal{X}_{t,s}(\mathbf{u})$ denotes the error term. To estimate $\delta_s(\mathbf{u})$ and $\mathcal{X}_{t,s}(\mathbf{u})$, we consider the functional median polish of [Sun and Genton \(2012\)](#), due to its robustness to outliers.

The functional median polish extends the classical median polish procedure of [Emerson and](#)

Hoaglin (1983) to the functional data setting and retains robustness to outliers. As outlined in Sun and Genton (2012), the functional grand effect and row effects can be obtained through the following iterative procedure:

- 1) Compute the functional median for each row and record these values. Subtract the corresponding row functional median from each function within that row.
- 2) Compute the functional median of the row functional medians and denote it as the functional grand effect. Subtract this grand effect from each row's functional median, and record the resulting quantities as the functional row effects.
- 3) Repeat Steps 1) and 2), updating and accumulating the functional grand and row effects at each iteration, until the row functional medians stabilize and no further changes occur.

Alternatively, the mean-based functional ANOVA can also be considered. Computationally, it can be achieved via the `One_way_median_polish` function in the `hdfts` package (Shang, 2025) in [R](#).

3.2 A functional factor model

We revisit the matrix factor model to decompose a matrix $\mathbf{X}_{t,s}$ as:

$$\mathbf{X}_{t,s} = \sum_{k=1}^{k_*} \mathbf{B}_{k,s} F_{tk} + \varepsilon_{t,s}, \quad s = 1, 2, \dots, N, \quad t = 1, 2, \dots, T, \quad (1)$$

where $\mathbf{B}_{k,s}$ denotes the k^{th} factor loading, F_{tk} denotes the k^{th} factor, k_* denotes the number of factors, and $\varepsilon_{t,s}$ denotes the error term. Let $\mathbf{X}_t = (\mathbf{X}_{t,1}, \dots, \mathbf{X}_{t,N})^\top$, $\mathbf{F}_t = (F_{t,1}, \dots, F_{t,k_*})^\top$, $\boldsymbol{\varepsilon}_t = (\varepsilon_{t,1}, \dots, \varepsilon_{t,N})^\top$ and

$$\mathbf{B} = \begin{pmatrix} \mathbf{B}_{11} & \cdots & \mathbf{B}_{1k_*} \\ \vdots & \ddots & \vdots \\ \mathbf{B}_{N1} & \cdots & \mathbf{B}_{Nk_*} \end{pmatrix},$$

an $N \times k_*$ matrix. Expressing (1) in a matrix format,

$$\mathbf{X}_t = \mathbf{B}\mathbf{F}_t + \boldsymbol{\varepsilon}_t. \quad (2)$$

Equation (2) is a factor representation for matrix-valued time series.

To extend it to HDFTS, let $\mathbf{B}_{k,s}$ be a linear integral operator with kernel $(B_{k,s}(\mathbf{u}, \mathbf{v}) : \mathbf{u} \in \mathcal{C}_i, \mathbf{v} \in \mathcal{C}_k^*)$, expressed as

$$\mathbf{B}_{k,s}(f)(\mathbf{u}) = \int_{\mathcal{C}_k^*} B_{k,s}(\mathbf{u}, \mathbf{v})f(\mathbf{v})d\mathbf{v}, \quad f \in \mathcal{H}_k^*.$$

Equation (1) can be re-expressed as

$$\mathcal{X}_{t,s}(\mathbf{u}) = \sum_{k=1}^{k_*} \int_{\mathcal{C}_k^*} B_{k,s}(\mathbf{u}, \mathbf{v})F_{t,k}(\mathbf{v})d\mathbf{v} + \varepsilon_{t,s}(\mathbf{u}).$$

By imposing a low-dimensional functional factor condition on the latent factor $F_{t,k}(\mathbf{v})$, we obtain the series approximation

$$F_{t,k}(\mathbf{v}) = \Phi_k(\mathbf{v})^\top \mathbf{G}_t + \zeta_{t,k}(\mathbf{v}), \quad \mathbf{v} \in \mathcal{C}_k^*, \quad k = 1, \dots, k_*, \quad (3)$$

where $\Phi_k(\cdot)$ is a q -dimensional vector of basis functions, \mathbf{G}_t is a q -dimensional vector of stationary random variables, and $\zeta_{t,k}(\mathbf{v})$ is the approximation error.

By plugging (3) into (2), we obtain

$$\begin{aligned} \mathcal{X}_{t,s}(\mathbf{u}) &= \sum_{k=1}^{k_*} \int_{\mathcal{C}_k^*} B_{k,s}(\mathbf{u}, \mathbf{v}) [\Phi_k(\mathbf{v})^\top \mathbf{G}_t + \zeta_{t,k}(\mathbf{v})] d\mathbf{v} + \varepsilon_{t,s}(\mathbf{u}) \\ &= \sum_{k=1}^{k_*} \int_{\mathcal{C}_k^*} B_{k,s}(\mathbf{u}, \mathbf{v}) \Phi_k(\mathbf{v})^\top d\mathbf{v} \mathbf{G}_t + \sum_{k=1}^{k_*} \int_{\mathcal{C}_k^*} B_{k,s}(\mathbf{u}, \mathbf{v}) \zeta_{t,k}(\mathbf{v}) d\mathbf{v} + \varepsilon_{t,s}(\mathbf{u}) \\ &= \Lambda_s(\mathbf{u})^\top \mathbf{G}_t + \varepsilon_{t,s}^*(\mathbf{u}), \end{aligned} \quad (4)$$

where $\Lambda_s(\mathbf{u}) = \sum_{k=1}^{k_*} \int_{\mathcal{C}_k^*} B_{k,s}(\mathbf{u}, \mathbf{v}) \Phi_k(\mathbf{v})^\top d\mathbf{v}$ and $\varepsilon_{t,s}^*(\mathbf{u}) = \sum_{k=1}^{k_*} \int_{\mathcal{C}_k^*} B_{k,s}(\mathbf{u}, \mathbf{v}) \zeta_{t,k}(\mathbf{v}) d\mathbf{v} + \varepsilon_{t,s}(\mathbf{u})$.

To estimate $\widehat{\mathbf{G}}_t$, we begin with the estimation of the covariance of $\mathcal{X}_{t,s}(\mathbf{u})$ by

$$\mathbf{\Delta} = (\Delta_{tt'})_{T \times T} \quad \text{with} \quad \Delta_{tt'} = \frac{1}{N} \sum_{s=1}^N \int_{\mathbf{u} \in \mathcal{C}_s} \mathcal{X}_{t,s}(\mathbf{u}) \mathcal{X}_{t',s}(\mathbf{u}) d\mathbf{u}.$$

Via the eigenanalysis of the $T \times T$ matrix $\mathbf{\Delta}$, we obtain $\widetilde{\mathbf{G}} = (\widetilde{\mathbf{G}}_1, \dots, \widetilde{\mathbf{G}}_T)^\top$ as a $T \times q$ matrix with columns being the eigenvectors (multiplied by \sqrt{T}) corresponding to the q largest estimated

eigenvalues of Δ , where q is a proxy of k_* in (4). The factor loading functions are estimated as

$$\tilde{\Lambda}_s(\mathbf{u}) = (\tilde{\Lambda}_s(\mathbf{u}) : \mathbf{u} \in \mathcal{C}_s) = \frac{1}{T} \sum_{t=1}^T x_{t,s}(\mathbf{u}) \tilde{\mathbf{G}}_t, \quad s = 1, \dots, N,$$

via the least-squares, using the normalization restriction $\frac{1}{T} \sum_{t=1}^T \tilde{\mathbf{G}}_t \tilde{\mathbf{G}}_t^\top = \mathbf{I}_q$ and \mathbf{I}_q is an identity matrix of dimension q .

To estimate q , we consider an information criterion, introduced in [Leng et al. \(2026\)](#), to estimate the factor number q , which can slowly diverge to infinity. Let $\nu_\ell(\Delta/T)$ be the ℓ^{th} largest eigenvalue of Δ/T and define

$$\hat{q} = \arg \min_{1 \leq \ell \leq q_{\max}} [\nu_\ell(\Delta/T) + \ell \cdot \phi_{N,T}] - 1,$$

where $\phi_{N,T}$ is the penalty parameter and q_{\max} is a user-specific positive integer. In practice, we set $\phi_{N,T} = [\max(T, N)]^{-\frac{1}{2}}$, and $q_{\max} = T$.

4 Conformal prediction

4.1 Split conformal prediction

We partition the 49-year sample (1975–2023) into training, validation, and test sets with proportions of 60%, 20%, and 20%, respectively. Using the initial training period from 1975 to 2002, we adopt an expanding-window forecasting scheme to generate h -step-ahead forecasts for the validation period 2003–2013, for $h = 1, 2, \dots, 10$ (see also [Shang and Haberman, 2026](#), for a functional time series). Under this scheme, the training sample is progressively enlarged at each iteration. The number of available curves in the validation or test set varies with the forecast horizon h : for instance, when $h = 1$, there are 11 years to compute residual functions, whereas when $h = 10$, only two years are available, corresponding to the differences between the observed curves in the validation set and their forecasts. From these residual functions, we compute pointwise summary measures $\gamma_s(\mathbf{u})$ for each prefecture s , such as the pointwise standard deviation. Alternatively, for quantile-based intervals, we take the absolute residuals and calculate the $100(1 - \alpha)\%$ empirical quantile, where α is the significance level, typically $\alpha = 0.05$ (see also [Shang and Hernandez, 2025](#)).

For a given horizon h , denote the residual functions by $\hat{\varepsilon}_{m,s}(\mathbf{u}) = Z_{m,s}(\mathbf{u}) - \hat{Z}_{m,s}(\mathbf{u})$ for $m = 1, \dots, M$, where M is the number of years in the validation set. Our objective is to determine a tuning parameter ξ_α such that $100(1 - \alpha)\%$ of the residuals satisfy

$$-\xi_\alpha \gamma_s(\mathbf{u}) \leq \hat{\varepsilon}_{m,s}(\mathbf{u}) \leq \xi_\alpha \gamma_s(\mathbf{u}).$$

By the law of large numbers, when M is reasonably large, one could achieve

$$\Pr \left[-\xi_\alpha \gamma_s(\mathbf{u}) \leq Z_{T+h,s}(\mathbf{u}) - \hat{Z}_{T+h,s}(\mathbf{u}) \leq \xi_\alpha \gamma_s(\mathbf{u}) \right] \approx \frac{1}{M} \sum_{m=1}^M \mathbb{1} \{ -\xi_\alpha \gamma_s(\mathbf{u}) \leq \hat{\varepsilon}_{m,s}(\mathbf{u}) \leq \xi_\alpha \gamma_s(\mathbf{u}) \},$$

where $Z_{T+h,s}(\mathbf{u})$ denotes the holdout age-specific mortality rates at time $T + h$ in prefecture s , $\hat{Z}_{T+h,s}(\mathbf{u})$ denotes the corresponding forecasts in the original scale (after taking exponential back-transformation), and $\mathbb{1}\{\cdot\}$ represents the binary indicator function.

4.2 Sequential conformal prediction

Without the need for a validation set, this sequential conformal prediction can automatically tune the predictive quantiles of the absolute residual functions as new data arrive. For instance, with the last 10 years as the test set, we use the other years to compute the absolute residuals $\{|e_3(\mathbf{u}_j)|, \dots, |e_t(\mathbf{u}_j)|\}$ for a given age \mathbf{u}_j . We require at least the first two curves to produce a forecast, so residuals begin with the 3rd curve.

At the quantile of $1 - \alpha$, we fit a quantile regression on lagged residuals, where the order of autoregression, denoted by p , is determined by an information criterion, such as the Akaike information criterion. Conditional on the most recent p number of the absolute residuals as the input, we predict a one-step-ahead quantile, denoted as $\hat{q}_{t+1,\alpha}(\mathbf{u}_j)$, where t represents the data in the end of the training period. The prediction intervals are then given by

$$\hat{Z}_{t+1}(\mathbf{u}_j) \pm \hat{q}_{t+1,\alpha}(\mathbf{u}_j), \quad j = 1, \dots, J.$$

Once the actual curve $Z_{t+1}(\mathbf{u}_j)$ arrives, we can update the absolute residual $|e_{t+1}(\mathbf{u}_j)|$ and refit.

5 Evaluation of interval forecast accuracy

5.1 Expanding-window forecast scheme

We partition the Japanese age-specific mortality data into a training period (1975–2002), a validation period (2003–2013), and a test period (2014–2023). The 10-year test sample enables us to assess forecast horizons from $h = 1$ to 10, reflecting varying levels of forecast uncertainty; for a relatively smaller horizon, its forecast uncertainty is comparably smaller (see also [Shang and Haberman, 2026](#)). The validation period spans 11 years, as certain summary measures, such as quantiles or standard deviations, require at least two years of observations for reliable computation.

We adopt an expanding-window forecasting scheme, which is widely used in time-series analysis to evaluate model adequacy and parameter stability over time (see [Zivot and Wang, 2006](#), Chapter 9). Specifically, using the initial 28 years (1975–2002), we generate one- to 10-step-ahead forecasts. The training sample is then expanded to include 2003 (i.e., 1975–2003), the model parameters are re-estimated, and new one- to 10-step-ahead forecasts are produced. This procedure continues recursively, increasing the sample size by one year at each step until the end of the observation period in 2023. As a result, we obtain 10 one-step-ahead forecasts, 9 two-step-ahead forecasts, and so on, up to a single 10-step-ahead forecast. Figure 4 illustrates the expanding-window scheme for the case $h = 1$, while similar procedures are applied for forecast horizons $h = 2, \dots, 10$.

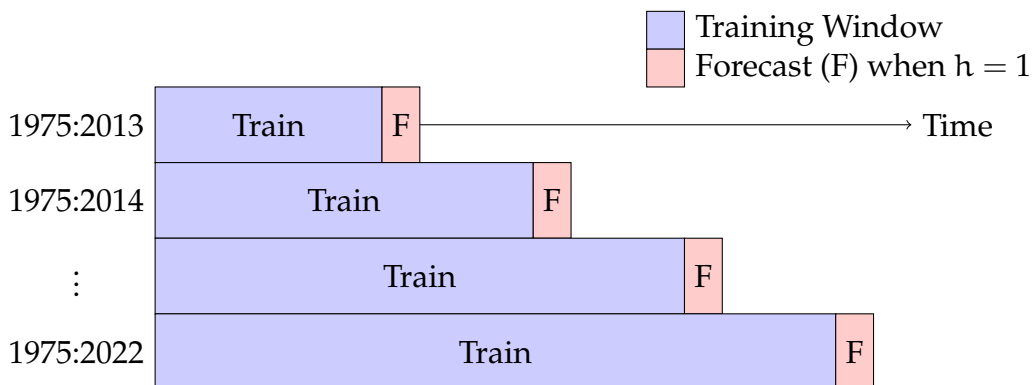


Figure 3: A diagram of the expanding-window forecast scheme, for the observations in the test set. The same scheme is also applied to calibrate tuning parameters using a validation set in the split conformal prediction method. In the forecast accuracy evaluation, we consider forecast horizon $h = 1, 2, \dots, 10$.

5.2 Measure of interval forecast accuracy

To evaluate and compare interval forecast accuracy, we consider the empirical coverage probability (ECP), the coverage probability difference (CPD), and the interval score of [Gneiting and Raftery \(2007\)](#). For each year in the test set, the h -step-ahead prediction intervals are calculated at the $1 - \alpha$ nominal coverage probability, the lower and upper bounds, denoted by $[\hat{z}_{\eta+\xi}^{\text{lb}}(\mathbf{u}), \hat{z}_{\eta+\xi}^{\text{ub}}(\mathbf{u})]$, are not required to be centered around the point forecasts (see also [Jiménez-Varón et al., 2024](#); [Shang and Haberman, 2026](#)). The ECP and CPD are defined as

$$\text{ECP}_h = \frac{1}{101 \times (11 - h)} \sum_{\xi=h}^{10} \sum_{j=1}^{101} \mathbb{1} \left\{ \hat{z}_{\eta+\xi}^{\text{lb}}(\mathbf{u}_j) \leq z_{\eta+\xi}(\mathbf{u}_j) \leq \hat{z}_{\eta+\xi}^{\text{ub}}(\mathbf{u}_j) \right\},$$

$$\text{CPD}_h = \left| \frac{1}{101 \times (11 - h)} \sum_{\xi=h}^{10} \sum_{j=1}^{101} \left[\mathbb{1}\{z_{\eta+\xi}(\mathbf{u}_j) > \hat{z}_{\eta+\xi}^{\text{ub}}(\mathbf{u}_j)\} + \mathbb{1}\{z_{\eta+\xi}(\mathbf{u}_j) < \hat{z}_{\eta+\xi}^{\text{lb}}(\mathbf{u}_j)\} \right] - \alpha \right|,$$

where η represents the jump-off year, which is the base year from which forecasts are computed.

The ECP assesses coverage without evaluating the sharpness of the prediction interval. By combining the coverage and sharpness, we consider a scoring rule for the prediction interval at age \mathbf{u}_j , defined as

$$\begin{aligned} S_{\alpha,\xi}[\hat{z}_{\eta+\xi,s}^{\text{lb}}(\mathbf{u}_j), \hat{z}_{\eta+\xi,s}^{\text{ub}}(\mathbf{u}_j), z_{\eta+\xi}(\mathbf{u}_j)] &= \left[\hat{z}_{\eta+\xi,s}^{\text{ub}}(\mathbf{u}_j) - \hat{z}_{\eta+\xi,s}^{\text{lb}}(\mathbf{u}_j) \right] \\ &+ \frac{2}{\alpha} \left[\hat{z}_{\eta+\xi,s}^{\text{lb}}(\mathbf{u}_j) - z_{\eta+\xi}(\mathbf{u}_j) \right] \mathbb{1} \left\{ z_{\eta+\xi}(\mathbf{u}_j) < \hat{z}_{\eta+\xi,s}^{\text{lb}}(\mathbf{u}_j) \right\} \\ &+ \frac{2}{\alpha} \left[z_{\eta+\xi}(\mathbf{u}_j) - \hat{z}_{\eta+\xi,s}^{\text{ub}}(\mathbf{u}_j) \right] \mathbb{1} \left\{ z_{\eta+\xi}(\mathbf{u}_j) > \hat{z}_{\eta+\xi,s}^{\text{ub}}(\mathbf{u}_j) \right\}. \end{aligned}$$

Averaging over the number of ages and the number of years in the testing set, the mean interval score is given as

$$\bar{S}_{\alpha,h} = \frac{1}{101 \times (11 - h)} \sum_{\xi=h}^{10} \sum_{j=1}^{101} S_{\alpha,\xi} \left[\hat{z}_{\eta+\xi,s}^{\text{lb}}(\mathbf{u}_j), \hat{z}_{\eta+\xi,s}^{\text{ub}}(\mathbf{u}_j), z_{\eta+\xi}(\mathbf{u}_j) \right].$$

Given the same ECP, the mean interval score rewards narrower prediction intervals. It is the other criterion used for comparing interval forecast accuracy.

6 Evaluating interval forecast accuracy

In Table 1, we present one-to-10-step-ahead interval forecast accuracy results between the two variants of conformal prediction, under the nominal coverage probability of 95%. The split conformal prediction tends to *underestimate* the coverage probability where the ECP is smaller than the nominal one. In contrast, the sequential conformal prediction tends to *overestimate* the coverage. Between the two summary statistics in split conformal prediction, the standard deviation is our recommended choice, as it allows calibration of the coverage using a validation set. Such a calibration is especially helpful with a larger forecast horizon.

Table 1: Averaged over 47 prefectures by age and sex in Japan, we present the one-to 10-step-ahead interval forecast accuracy for the two variants of conformal prediction, namely split and sequential conformal predictions, at the nominal coverage probability of 95%. In split conformal prediction, we consider two summary statistics: the standard deviation (sd) and the quantile. For forecasting principal component scores, we consider two univariate time-series forecasting methods, namely the autoregressive integrated moving average (ARIMA) and exponential smoothing (ETS).

Method	Sex	h	Split (sd)			Split (quantile)			Sequential		
			ECP	CPD	score	ECP	CPD	score	ECP	CPD	score
ARIMA	F	1	0.934	0.022	0.008	0.894	0.058	0.007	0.969	0.029	0.013
		2	0.928	0.029	0.009	0.879	0.073	0.009	0.971	0.031	0.014
		3	0.919	0.035	0.010	0.849	0.103	0.010	0.974	0.030	0.015
		4	0.915	0.040	0.011	0.832	0.120	0.011	0.975	0.031	0.016
		5	0.901	0.052	0.014	0.799	0.153	0.014	0.976	0.032	0.018
		6	0.896	0.057	0.017	0.774	0.178	0.016	0.974	0.032	0.019
		7	0.903	0.052	0.019	0.748	0.205	0.017	0.971	0.031	0.020
		8	0.924	0.031	0.019	0.738	0.214	0.015	0.970	0.030	0.022
		9	0.943	0.018	0.022	0.727	0.225	0.013	0.969	0.029	0.024
		10	0.931	0.028	0.083	0.645	0.305	0.014	0.968	0.028	0.025
		Mean	0.919	0.036	0.021	0.788	0.164	0.013	0.972	0.030	0.019
	M	1	0.941	0.017	0.014	0.908	0.044	0.013	0.980	0.032	0.021
2		0.935	0.021	0.014	0.897	0.056	0.014	0.981	0.033	0.021	
3		0.931	0.025	0.015	0.884	0.068	0.015	0.984	0.034	0.022	

Continued on next page

Method	Sex	h	ECP	CPD	score	ECP	CPD	score	ECP	CPD	score
		4	0.926	0.029	0.016	0.870	0.082	0.016	0.987	0.037	0.023
		5	0.921	0.033	0.017	0.848	0.104	0.018	0.989	0.039	0.025
		6	0.916	0.039	0.019	0.828	0.125	0.020	0.989	0.039	0.026
		7	0.913	0.043	0.023	0.801	0.151	0.025	0.990	0.040	0.027
		8	0.917	0.040	0.027	0.766	0.186	0.028	0.991	0.041	0.028
		9	0.925	0.033	0.036	0.707	0.246	0.036	0.993	0.043	0.029
		10	0.923	0.032	0.102	0.614	0.336	0.047	0.993	0.043	0.030
		Mean	0.925	0.031	0.028	0.812	0.140	0.023	0.988	0.038	0.025
ETS	F	1	0.935	0.022	0.008	0.890	0.063	0.007	0.967	0.029	0.013
		2	0.930	0.027	0.009	0.875	0.077	0.008	0.969	0.029	0.014
		3	0.926	0.030	0.010	0.858	0.095	0.009	0.972	0.029	0.015
		4	0.925	0.031	0.010	0.847	0.106	0.009	0.976	0.031	0.016
		5	0.922	0.033	0.010	0.825	0.127	0.010	0.977	0.032	0.018
		6	0.923	0.034	0.012	0.806	0.147	0.011	0.975	0.031	0.020
		7	0.919	0.039	0.014	0.780	0.172	0.012	0.971	0.030	0.020
		8	0.925	0.033	0.015	0.748	0.204	0.013	0.970	0.031	0.022
		9	0.928	0.031	0.021	0.695	0.258	0.018	0.970	0.030	0.022
		10	0.904	0.053	0.051	0.589	0.361	0.026	0.967	0.025	0.023
		Mean	0.924	0.033	0.016	0.791	0.161	0.012	0.971	0.030	0.018
	M	1	0.945	0.015	0.014	0.912	0.041	0.012	0.979	0.031	0.020
		2	0.943	0.017	0.014	0.905	0.047	0.013	0.980	0.032	0.021
		3	0.940	0.019	0.015	0.892	0.060	0.013	0.982	0.033	0.022
		4	0.941	0.021	0.016	0.880	0.072	0.015	0.984	0.035	0.023
		5	0.939	0.024	0.017	0.863	0.089	0.017	0.986	0.036	0.024
		6	0.949	0.020	0.017	0.855	0.098	0.017	0.987	0.037	0.026
		7	0.951	0.022	0.019	0.845	0.106	0.019	0.987	0.037	0.026
		8	0.956	0.021	0.022	0.822	0.130	0.021	0.988	0.038	0.027
		9	0.962	0.020	0.037	0.795	0.158	0.026	0.990	0.040	0.028
		10	0.931	0.033	0.114	0.731	0.219	0.030	0.994	0.044	0.028
		Mean	0.946	0.021	0.029	0.850	0.102	0.018	0.986	0.036	0.025

Between the split conformal prediction (sd) and sequential conformal prediction, we display one- to 10-step-ahead ECPs in Figure 4. For each horizon, we present a boxplot of ECPs from the 47 prefectures. For the split conformal prediction, there is a tendency to under-estimate the coverage probability, especially from $h = 3$ to $h = 7$. Such an underestimation is likely because the calibration in the validation set may not be optimal for the data in the test set. In contrast, the sequential conformal prediction often overestimates the coverage probability and tends to be conservative.

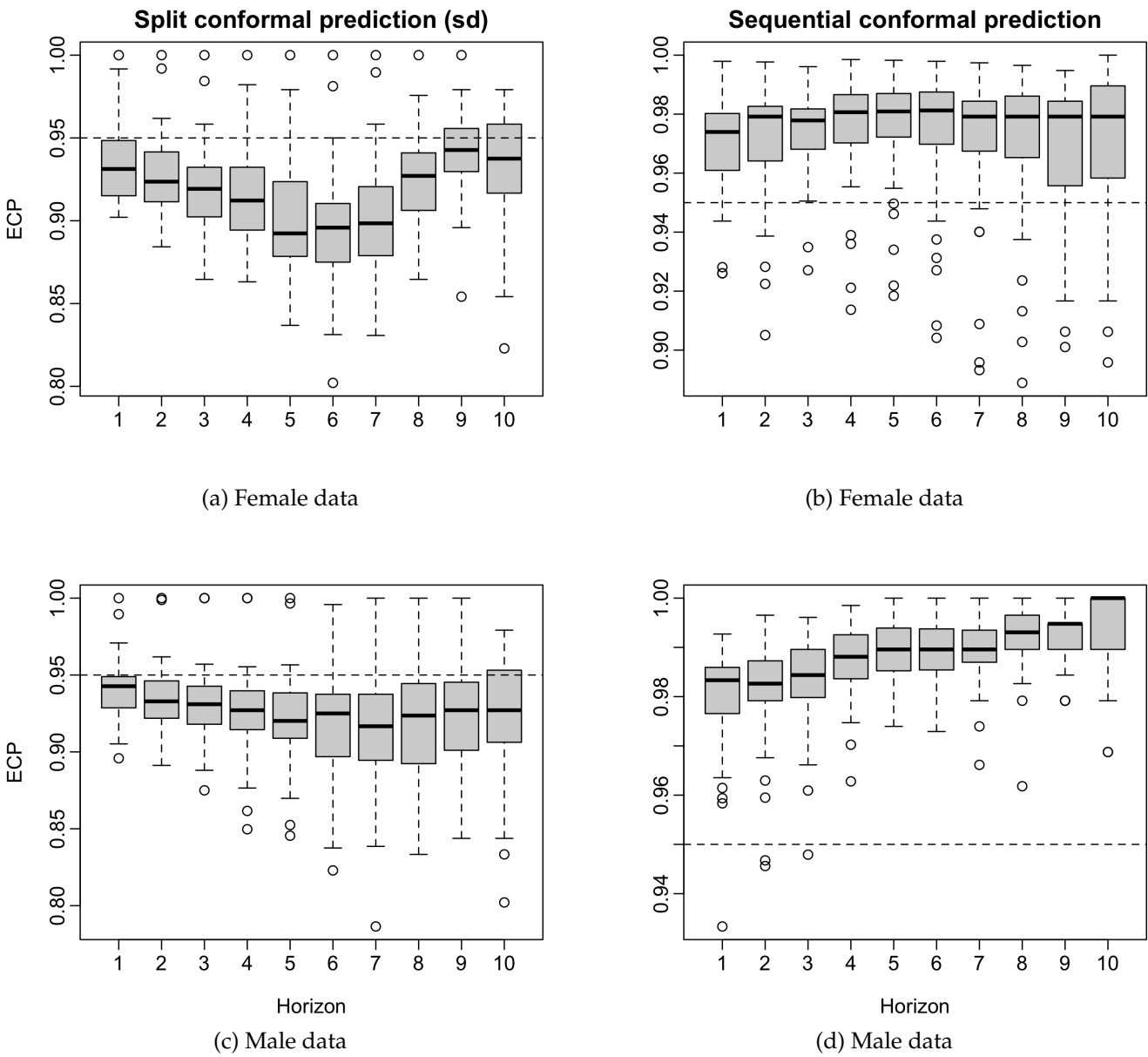


Figure 4: For forecast horizon $h = 1, 2, \dots, 10$, a comparison of the ECPs of the female and male data between the split and sequential conformal predictions at the nominal coverage probability of 95%. Each boxplot contains the ECP values from the 47 prefectures.

In Figure 5, we further present one- to 10-step-ahead mean interval scores between the split conformal prediction and sequential conformal prediction. The sequential conformal prediction achieves lower mean interval scores than those from the split conformal prediction. It highlights the unparallel trade-off between coverage and sharpness. Under a level of significance $\alpha = 0.05$, it seems to be beneficial to overestimate the coverage probability rather than underestimate it.

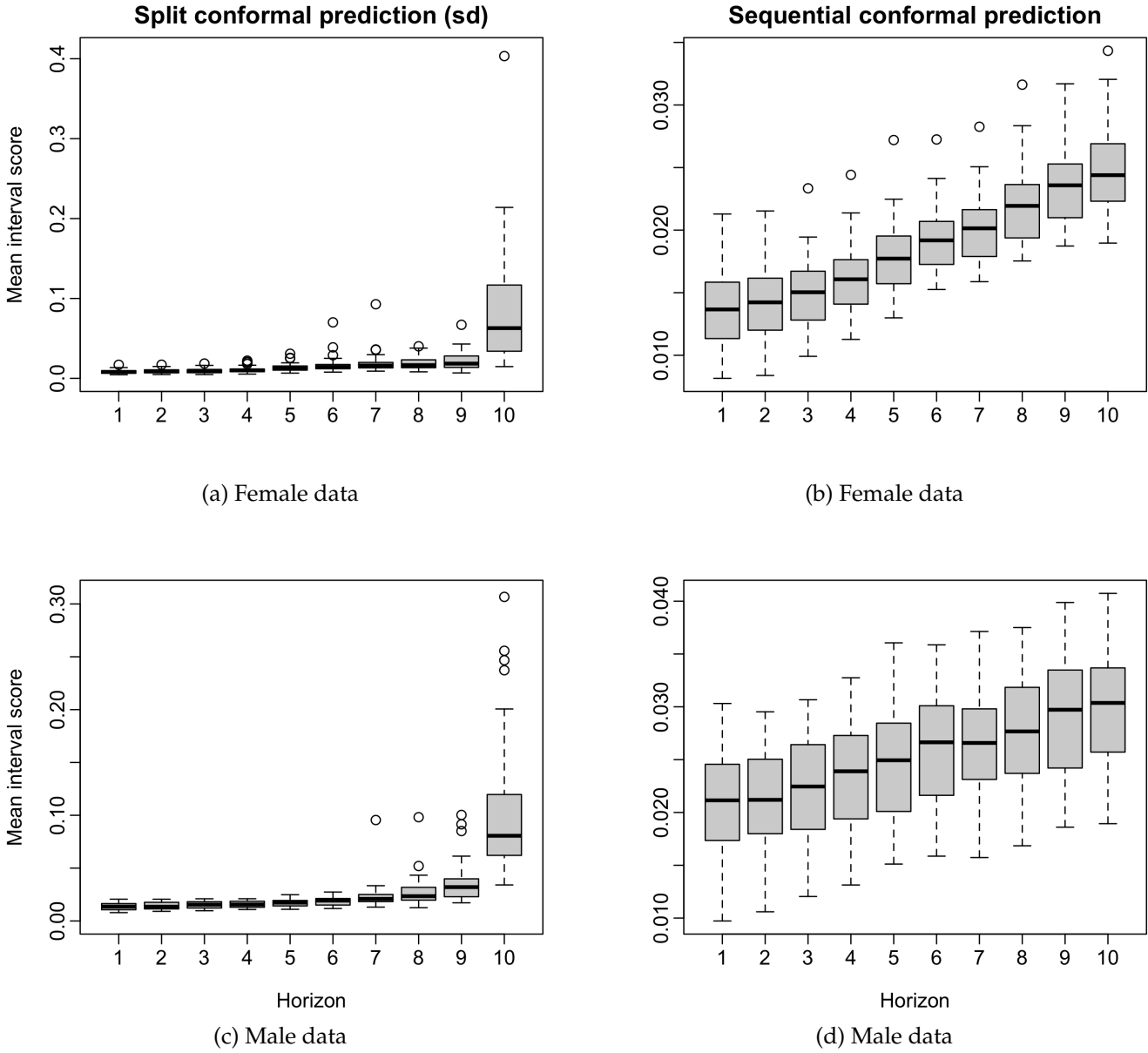


Figure 5: For forecast horizon $h = 1, 2, \dots, 10$, a comparison of the mean interval scores of the female and male data between the split and sequential conformal predictions. Each boxplot contains the mean interval scores from the 47 prefectures. For the split conformal prediction, the relatively larger mean interval score is because there are only a few data curves for calibration in the validation set for a relatively large forecast horizon.

7 Conclusion

We present conformal prediction as a means to quantify forecast uncertainty for high-dimensional functional time series and demonstrate its usage using Japanese subnational age- and sex-specific log mortality rates from 1975 to 2023. The conformal prediction framework is model-agnostic and distribution-free to construct prediction intervals. Using a one-way functional analysis of variance and a functional factor model, we evaluate and compare the finite-sample performance between split and sequential conformal predictions. To facilitate reproducibility, the  code for computing the interval forecast errors obtained from the split and sequential conformal predictions using the Japanese and Canadian mortality data is available at https://github.com/hanshang/conformal_prediction_OWFANOVA_FFM.

Split conformal prediction requires sample splitting, which can lead to inferior interval forecast accuracy at longer forecast horizons. As a model-agnostic, tuning-parameter-free approach, the sequential conformal prediction gradually updates the predictive quantiles when new data arrive. Because it does not require calibration using a validation set, this conservative approach is recommended for quantifying finite-sample prediction uncertainty.

There are several ways in which the current paper may be further extended, and we briefly outline two: 1) In the sequential conformal prediction, we model the temporal dependence of the absolute residuals via an autoregressive process in a quantile regression. Other time-series models can also be applied. 2) Female and male data are modelled separately. For each sex, the observations form a three-dimensional array indexed by age, calendar year, and prefecture. Modeling both sexes jointly increases the effective dimensionality of the problem, thereby requiring more sophisticated statistical tools to decompose and analyze such data. In this setting, approaches, such as two-way functional analysis of variance studied in [Jiménez-Varón et al. \(2024\)](#), coupled with functional factor models, provide natural and flexible frameworks.

Acknowledgment

This research is financially supported by the Australian Research Council Discovery Project DP230102250 and Australian Research Council Future Fellowship FT240100338.

Disclosure statement

No potential conflict of interest was reported by the author.

Appendix: Canadian subnational age- and sex-specific mortality

As a sensitivity analysis, we also consider age-specific log mortality data for 12 Canadian provinces and territories, obtained from the Canadian Human Mortality Database (<http://www.bdlc.umontreal.ca/chmd/>). For most regions, observations are available through 2023, except for Yukon. For consistency and completeness across regions, we restrict the study period to 1950–2016. To mitigate the impact of measurement error at advanced ages, ages are grouped from 0 to 79 in single-year intervals, with ages 80 and above aggregated into an open-ended age group. Using the same experimental design and error metric as in Section 5, we apply both split and sequential conformal predictions to evaluate and compare the accuracy of interval forecasts in Table 2.

Table 2: Averaged over 47 prefectures by age and sex in Japan, we present the one-to 10-step-ahead interval forecast accuracy for the two variants of conformal prediction, namely split and sequential conformal predictions, at the nominal coverage probability of 95%. In split conformal prediction, we consider two summary statistics: the standard deviation (sd) and the quantile. For forecasting principal component scores, we consider the ARIMA and ETS methods.

Method	Sex	h	Split (sd)			Split (quantile)			Sequential		
			ECP	CPD	score	ECP	CPD	score	ECP	CPD	score
ARIMA	F	1	0.938	0.012	0.033	0.867	0.083	0.011	0.992	0.043	0.023
		2	0.930	0.021	0.031	0.856	0.094	0.011	0.993	0.043	0.023

Continued on next page

Method	Sex	h	ECP	CPD	score	ECP	CPD	score	ECP	CPD	score
		3	0.926	0.024	0.031	0.842	0.108	0.011	0.993	0.043	0.024
		4	0.922	0.028	0.031	0.831	0.119	0.012	0.994	0.044	0.024
		5	0.918	0.032	0.033	0.805	0.145	0.013	0.994	0.044	0.024
		6	0.911	0.039	0.036	0.781	0.169	0.014	0.994	0.044	0.024
		7	0.914	0.037	0.036	0.765	0.185	0.014	0.996	0.046	0.024
		8	0.918	0.034	0.063	0.716	0.234	0.015	0.994	0.044	0.024
		9	0.884	0.066	0.035	0.661	0.289	0.016	0.995	0.045	0.025
		10	0.847	0.108	0.074	0.575	0.375	0.026	0.994	0.044	0.025
		Mean	0.911	0.040	0.040	0.770	0.180	0.014	0.994	0.044	0.024
	M	1	0.941	0.015	0.036	0.909	0.041	0.013	0.990	0.042	0.019
		2	0.937	0.017	0.037	0.906	0.045	0.013	0.991	0.043	0.020
		3	0.937	0.018	0.035	0.899	0.052	0.013	0.992	0.042	0.020
		4	0.940	0.018	0.038	0.886	0.064	0.013	0.991	0.041	0.020
		5	0.943	0.021	0.036	0.869	0.081	0.014	0.991	0.041	0.021
		6	0.938	0.022	0.037	0.857	0.093	0.014	0.991	0.041	0.021
		7	0.939	0.029	0.487	0.835	0.115	0.015	0.992	0.042	0.021
		8	0.944	0.023	0.053	0.816	0.134	0.016	0.993	0.043	0.021
		9	0.920	0.047	0.052	0.763	0.187	0.018	0.991	0.041	0.021
		10	0.872	0.084	0.093	0.702	0.248	0.022	0.988	0.040	0.022
		Mean	0.931	0.029	0.090	0.844	0.106	0.015	0.991	0.042	0.021
ETS	F	1	0.937	0.014	0.031	0.875	0.075	0.011	0.991	0.042	0.022
		2	0.932	0.018	0.031	0.864	0.086	0.011	0.992	0.042	0.022
		3	0.930	0.020	0.030	0.856	0.094	0.011	0.991	0.043	0.023
		4	0.930	0.020	0.031	0.849	0.101	0.012	0.991	0.043	0.024
		5	0.927	0.023	0.034	0.828	0.122	0.013	0.992	0.044	0.025
		6	0.927	0.024	0.037	0.817	0.133	0.012	0.993	0.044	0.025

Continued on next page

Method	Sex	h	ECP	CPD	score	ECP	CPD	score	ECP	CPD	score
		7	0.926	0.028	0.036	0.804	0.146	0.012	0.994	0.045	0.025
		8	0.927	0.027	0.072	0.769	0.181	0.013	0.997	0.047	0.025
		9	0.889	0.061	0.036	0.711	0.239	0.014	0.993	0.043	0.026
		10	0.889	0.063	0.167	0.614	0.336	0.023	0.995	0.045	0.026
		Mean	0.922	0.030	0.050	0.799	0.151	0.013	0.993	0.044	0.024
M		1	0.939	0.019	0.030	0.910	0.040	0.013	0.990	0.043	0.019
		2	0.939	0.015	0.038	0.907	0.044	0.013	0.991	0.043	0.020
		3	0.939	0.019	0.035	0.899	0.051	0.013	0.993	0.043	0.020
		4	0.942	0.018	0.041	0.885	0.065	0.013	0.992	0.043	0.020
		5	0.942	0.023	0.036	0.867	0.083	0.014	0.991	0.041	0.020
		6	0.939	0.024	0.037	0.857	0.093	0.014	0.993	0.043	0.020
		7	0.930	0.029	0.034	0.833	0.117	0.015	0.993	0.043	0.021
		8	0.947	0.025	0.053	0.812	0.138	0.016	0.993	0.043	0.021
		9	0.918	0.050	0.052	0.762	0.188	0.018	0.992	0.042	0.021
		10	0.883	0.074	0.094	0.704	0.246	0.022	0.988	0.038	0.021
		Mean	0.932	0.030	0.045	0.844	0.106	0.015	0.992	0.042	0.020

Consistent with earlier findings, split conformal prediction tends to underestimate the empirical coverage, whereas sequential conformal prediction tends to overestimate it. Notably, this overestimation is advantageous, as it results in smaller mean interval scores.

References

- Basellini, U. and Camarda, C. G. (2019), 'Modelling and forecasting adult age-at-death distributions', *Population Studies* **73**, 119–138.
- Chatfield, C. (2000), *Time-Series Forecasting*, Chapman & Hall, Boca Raton, Florida.
- Cuesta-Albertos, J. A. and Febrero-Bande, M. (2010), 'A simple multiway ANOVA for functional data', *Test* **19**, 537–557.
- Emerson, J. D. and Hoaglin, D. C. (1983), Analysis of two-way tables by medians, *in* D. C. Hoaglin, F. Mosteller and J. W. Tukey, eds, 'Understanding Robust and Exploratory Data Analysis', John Wiley & Sons, New York.
- Gao, Y., Shang, H. L. and Yang, Y. (2019), 'High-dimensional functional time series forecasting: An application to age-specific mortality rates', *Journal of Multivariate Analysis* **170**, 232–243.
- Gneiting, T. and Raftery, A. E. (2007), 'Strictly proper scoring rules, prediction and estimation', *Journal of the American Statistical Association: Review Article* **102**(477), 359–378.
- Guo, S., Qiao, X., Wang, Q. and Wang, Z. (2026), 'Factor modeling for high-dimensional functional time series', *Journal of Business and Economic Statistics* **44**(1), 106–119.
- Hallin, M., Nisol, G. and Tavakoli, S. (2023), 'Factor models for high-dimensional functional time series i: Representation results', *Journal of Time Series Analysis* **44**, 578–600.
- Happ, C. and Greven, S. (2018), 'Multivariate functional principal component analysis for data observed on different (dimensional) domains', *Journal of the American Statistical Association: Theory and Methods* **113**(522), 649–659.
- Hyndman, R. (2025), *demography: Forecasting Mortality, Fertility, Migration and Population Data*. R package version 2.0.1.
URL: <https://CRAN.R-project.org/package=demography>
- Hyndman, R. J. and Shang, H. L. (2010), 'Rainbow plots, bagplots, and boxplots for functional data', *Journal of Computational and Graphical Statistics* **19**(1), 29–45.

- Japanese Mortality Database (2026), *National Institute of Population and Social Security Research*. Available at <https://www.ipss.go.jp/p-toukei/JMD/index-en.asp> (data downloaded on January 28, 2026).
- Jiménez-Varón, C. F., Sun, Y. and Shang, H. L. (2024), 'Forecasting high-dimensional functional time series: Application to sub-national age-specific mortality', *Journal of Computational and Graphical Statistics* **33**(4), 1160–1174.
- Lei, J., G'Sell, M., Rinaldo, A., Tibshirani, R. J. and Wasserman, L. (2018), 'Distribution-free predictive inference for regression', *Journal of the American Statistical Association: Theory and Methods* **113**(523), 1094–1111.
- Leng, C., Li, D., Shang, H. L. and Xia, Y. (2026), 'Covariance function estimation for high-dimensional functional time series with dual factor structures', *Journal of Business & Economic Statistics* **in press**.
- Li, D., Li, R. and Shang, H. L. (2024), 'Detection and estimation of structural breaks in high-dimensional functional time series', *The Annals of Statistics* **52**(4), 1716–1740.
- Paparoditis, E. and Shang, H. L. (2023), 'Bootstrap prediction bands for functional time series', *Journal of the American Statistical Association: Theory and Methods* **118**(542), 972–986.
- Shang, H. L. (2025), *hdftsa: High-Dimensional Functional Time Series Analysis*. R package version 1.0.
URL: <https://CRAN.R-project.org/package=hdftsa>
- Shang, H. L. and Haberman, S. (2026), 'Constructing prediction intervals for the age distribution of deaths', *Scandinavian Actuarial Journal* **in press**.
- Shang, H. L. and Hernandez, I. M. (2025), 'Forecasting intraday particle number size distribution: A functional time-series approach', *Environmental and Ecological Statistics* **32**, 1313–1338.
- Smaga, L. (2026), 'Review of methods for functional one-way analysis of variance', *REVSTAT-Statistical Journal* **in press**.
- Sun, Y. and Genton, M. G. (2012), 'Functional median polish', *Journal of Agricultural, Biological, and Environmental Statistics* **17**(3), 354–376.

- Tavakoli, S., Nisol, G. and Hallin, M. (2023), 'Factor models for high-dimensional functional time series ii: Estimation and forecasting', *Journal of Time Series Analysis* **44**, 601–621.
- Wood, S. N. (1994), 'Monotonic smoothing splines fitted by cross validation', *SIAM Journal on Scientific Computing* **15**, 1126–1133.
- Xu, C. and Xie, Y. (2023), Sequential predictive conformal inference for time series, Working paper, arXiv.
URL: <https://arxiv.org/abs/2212.03463>
- Yang, Y., Shang, H. L. and Raymer, J. (2024), 'Forecasting Australian fertility by age, region, and birthplace', *International Journal of Forecasting* **40**(2), 532–548.
- Zivot, E. and Wang, J. (2006), *Modeling Financial Time Series with S-PLUS*, Vol. 2, Springer, New York.